Original Article

Institution of MECHANICAL ENGINEERS

Journal of MATERIALS: DESIGN AND APPLICATIONS

Application of Computational Fluid Dynamics to study the effects of Sprue Base Geometry on the Surface and Internal Turbulence in gravity casting

Proc IMechE Part L: J Materials: Design and Applications
0(0) 1–11

DOI: 10.1177/1464420713500182
pil.sagepub.com
SAGE

Amir Baghani[1], Ahmad Bahmani[1], Parviz Davami[1], Naser Varahram[1] and Mohsen Ostad Shabani[2]

Abstract

The effects of sprue base size and design on flow pattern during aluminum gravity casting have been investigated by employing different sprue base sizes and using computational fluid dynamics. Calculations were carried out using SUTCAST simulation software based on solving Navier–Stokes equation and tracing the free surface using SOLA-volume of fluid algorithm. Flow pattern was analyzed with focus on streamlines and velocity distribution in sprue base, runner and ingate. Increasing well size produced a vortex flow at the bottom of sprue base, which increased the surface velocity of liquid metal in runner. Using a rather big sprue well could eliminate vena contracta but ingate velocity was observed to be independent of well size. It is assumed that ingate velocity may be more influenced by other casting considerations. Using a curved sprue base could remove vortex flow at the bottom of sprue while keeping a nearly full contact between liquid metal and runner wall.

Keywords

Computational fluid dynamics, casting, Navier–Stokes

Date received: 12 February 2013; accepted: 11 July 2013

Introduction

A most important aspect of production of clean and sound castings is the method by which the molten metal is introduce into the mold cavity. One of the duties of the running and gating system is to ensure that the flow of metal should be as free as possible from turbulence but at a rate sufficient to avoid undue delay in filling the mold.[1] Surface turbulence promotes entrainment oxide films inside the cavity. Oxide films play a major role in the control of mechanical properties that are affected by gating system design. Liquid aluminum contacts the surrounding atmosphere containing oxygen and has a tendency to form an insoluble oxide film on the surface. Oxide cracks are formed as a result of surface turbulence or bubble trail damage and cause uncertainties in the static strength of castings. The application of process control has been suggested to avoid such uncertainties and to ensure that such defects are not introduced in the first place.[2]

There is a critical velocity at liquid metal front that is high enough to push the metal surface but if its inertia pressure is smaller or equal to surface tension, then any perturbation could be avoided in this condition. For example, the critical ingate velocity for liquid aluminum was determined to be 0.5 m s^{-1} by Campbell and Runyoro[3] and higher ingate velocities cause surface turbulence and generate severe rates of oxides entrainment. In an emphatic research, Kura and Grube[4] have investigated water flow through the transparent mold using a high frame per second camera. Maximum velocity of 0.457 m s^{-1} at the exit end of the gate has been captured and later while pouring liquid aluminum with 7% Mg at the same running system, no surface defects was observed in final product. Campbell and Green[5] has found that high-reliability aluminum alloy (Al-7Si-Mg) castings were obtained by bottom gating a sand mold at an initial gate velocity less than or equal to 0.5 m s^{-1}. The analysis also showed that the bottom

[1]Department of Material Science and Engineering, Sharif University of Technology, Tehran, Iran
[2]Materials and Energy Research Center (MERC), Karaj, Tehran, Iran

Corresponding author:
Amir Baghani, Razi Metallurgical Research Center, No.8, Fernan St., Sorkhehhesar Road, Km 21 Karadj Makhsous Road, Tehran, PO Box 14515-386, Iran.
Email: amir.baghani@gmail.com

gating at a velocity greater than the critical ingate velocity is equally as likely to produce bad castings as a top gating. It has also been pointed out that a poor running system design promoted the formation of large amounts of entrained folded oxide film defects, which reach low mechanical properties as low as ceramic material with weibull moduli in the range of 11–22. But modifying the running system reduced oxides defects with Weibull moduli in the range 38–54, which is close to those of aerospace forgings.[6] Campbell[7] has mentioned that if liquid aluminum drops a fairly short distance of 12.5 mm, the velocity has already reached its critical ingate velocity of 0.5 m s^{-1}, which could entrap insoluble films and generate bifilm defects.

Due to the importance of mold filling simulation and with aim of achieving a perfect sight of casting, extensive research efforts have been made to study the effect of gating design on the flow pattern of melt entering the mold.[8,9] In one of these studies, the effect of cross-sectional shapes of runner on the mechanical strength of Al-7Si-Mg alloy has investigated by Dai et al.[10] Their numerical and experimental results showed that the runner with circular cross-section is much more effective in keeping ingate velocity under critical velocity than one that has rectangular and triangular cross-section, thereby avoiding the generation of surface turbulence and the consequential entertainment oxide films.

It has been observed that if the cross-section of the runner after the filter is two times larger than that of the runner before the filter, the liquid metal could be in a permanent contact with the mold walls and slightly pressurized by it. In this condition, ceramic filter can play a major role in the reduction of velocity and the surface turbulence of the liquid metal in naturally pressurized systems.[11]

A diffusing runner system was proposed by Hsu and Lin[12] to reduce the velocity of liquid metal under critical velocity (0.5 m s^{-1} for Aluminum), while the flow rate remained almost unchanged. In order to investigate gate size effects on flow pattern, three gate dimension of 9×1, 4.5×2 and 6×1.5 (mm^2) were employed in a non-pressurized system for evaluating melt flow in a horizontal plate using direct observation method. It was found that increasing the thickness of the gate in a constant area will increase the pressure head at the gate exit, which could increase melt velocity.[13]

Besides all gating system portions, the design of a sprue base as a liquid plumbing system into the runner has received much attention from researchers over the years. When the metal has completed its controlled flow down the sprue, it moves at rather high velocities. Then, to introduce into the runner, it has to change direction and flow at a right angle relative to the sprue, causing splashing into the runner system. Again, this exposes large amounts of metal droplets to atmospheric conditions. Webster and Met[14] believed that by placing a small well at the bottom of the sprue, the molten metal can hit the bottom and lose excessive kinetic energy before entering the remaining portions of the gating system. Elliot[1] mentioned that the formation of vena contracta could be suppressed using a properly sized well that is able to reduce the surface turbulence.

Schwam et al.[15] have explained two melt flows generated as soon as the basin begins to fill. One is closer to the runner and proceeds into the mold and the other half begins to circulate in a "whirlpool" fashion. They analyzed that with the filled basin metal starts to forgo the basin and the flow acts as if no sprue well is present at all.

As indicated by Campbell,[2] after the well was filled, the rotation of the liquid in the well was seen to act as a kind of ball bearing, reducing the friction on the stream at the turn. In this manner, the velocity in the runner will increase. Moreover, contacting liquid metal with the runner when no well was used had the benefit of additional friction from the wall rather than using a well that caused useful reduction in metal speed.

The objective of this study is to investigate the effects of sprue base on flow pattern of liquid during mold filling using modeling based on computational fluid dynamics (CFD), focusing on the relationship among sprue base design, streamlines pattern and runner and ingate velocity distribution. Three gating systems were designed and the only difference between them was the size of the sprue bases and one gating system was designed with a curved sprue base. Streamlines and velocity distributions in different locations were analyzed precisely to evaluate the effect of sprue base on reduction of velocity, surface turbulence and formation of vena contracta.

Methods and procedures

Model selection

In order to evaluate different scales of sprue bases, a unpressurized system with different wells beneath the sprue was considered. The details of the dimensions of the four shapes is shown in Figure 1, including no well, standard sized well, over-sized well and no well with a curved sprue base. The dimensions of all molds and gating systems are identical except for sprue bases. Models include a sprue, sprue base, runner, gate and a rectangular casting part. This arrangement, similar for different molds except for sprue bases, allows for direct comparison of the behavior of liquid metal flow and performance of the castings acquired by using different sprue bases.

CFD model

In order to simulate the metal flow in gating systems with different sprue base, CFD modeling was

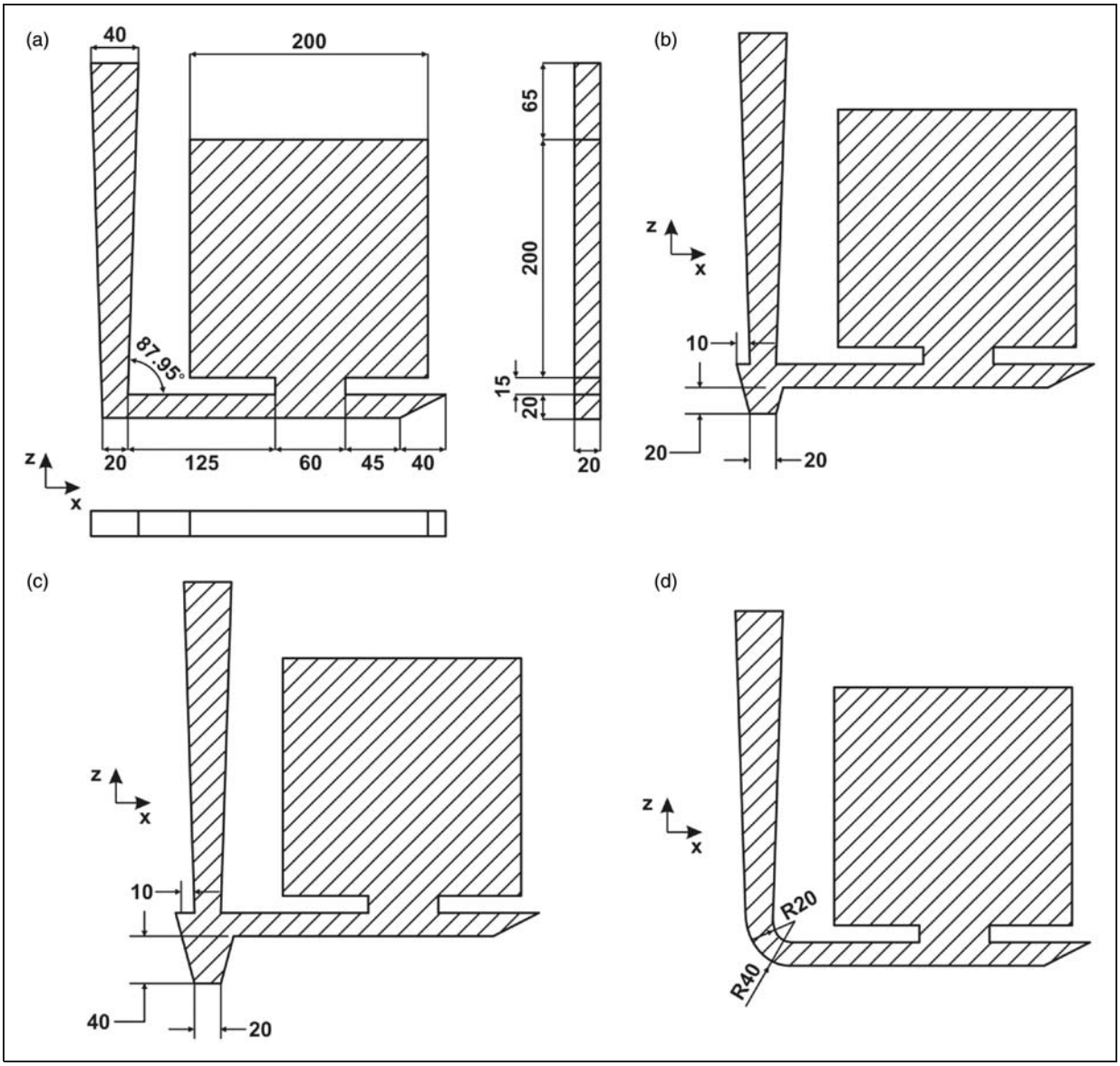

Figure 1. Different designs considered in this study to evaluate the behavior of mold filling with different sprue bases: (a) Model A with no sprue well, (b) Model B with standard sprue well, (c) Model C with large sprue well and (d) Model D with curved sprue base.

used.[16–20] This study employed the code SUTCAST. Non-iterative method of SOLA was employed to solve Navier–Stokes equation (equation (1))

$$\frac{\partial u}{\partial t} = -\vec{u}.\nabla u - \frac{\partial P}{\rho \partial x} + g_x + \frac{\mu}{\rho}\nabla^2 u$$

$$\frac{\partial v}{\partial t} = -\vec{u}.\nabla v - \frac{\partial P}{\rho \partial y} + g_y + \frac{\mu}{\rho}\nabla^2 v$$

$$\frac{\partial w}{\partial t} = -\vec{u}.\nabla w - \frac{\partial P}{\rho \partial z} + g_z + \frac{\mu}{\rho}\nabla^2 w \qquad (1)$$

where $\vec{u} = u\vec{i} + v\vec{j} + w\vec{k}$ is the velocity vector, g_x, g_y *and* g_z are the body acceleration components, ρ *and* μ represent density and viscosity, respectively (Table 1), and P is the liquid metal pressure.

Table 1. Aluminum A356 properties in pouring temperature of 720°C, employed in numerical simulation.

Density (kg m^{-3})	Viscosity (kg m s^{-1})
2390	0.01

Fluid velocities and pressures (in two dimensions) are located at cell positions, as shown in Figure 2; u and v-velocities are considered at the middle of the vertical and horizontal sides of the cell and pressure at the cell center.

The finite difference approximation of Navier–Stokes equations is

$$\begin{aligned}
u^{n+1}_{i+\frac{1}{2},j,k} &= u^{n}_{i+\frac{1}{2},j,k} + \delta t\left[-\frac{P^{n}_{i+1,j,k-}P^{n}_{i,j,k}}{\rho\delta x_{i+\frac{1}{2}}} + g_x - FUX - FUY - FUZ + VISX\right]\\
v^{n+1}_{i,j+\frac{1}{2},k} &= v^{n}_{i,j+\frac{1}{2},k} + \delta t\left[-\frac{P^{n}_{i,j+1,k-}P^{n}_{i,j,k}}{\rho\delta y_{j+\frac{1}{2}}} + g_y - FVX - FVY - FVZ + VISY\right]\\
w^{n+1}_{i,j,k+\frac{1}{2}} &= w^{n}_{i,j,k+\frac{1}{2}} + \delta t\left[-\frac{P^{n}_{i,j,k+1-}P^{n}_{i,j,k}}{\rho\delta z_{k+\frac{1}{2}}} + g_z - FWX - FWY - FWZ + VISZ\right]
\end{aligned} \tag{2}$$

In the above equation, advective flux (FUX) and viscosity term (VISX) in x-direction could be described as follows

$$\begin{aligned}
FUX &= \frac{u^{n}_{i+\frac{1}{2},j,k}}{\Delta x_{\alpha}}\Big[\Delta x_{i+1}.DUL + \Delta x_i.DUR + \alpha Sign\Big(u_{i+\frac{1}{2}}\Big)(\Delta x_{i+1}.DUL - \Delta x_i.DUR)\Big];\\
DUL &= \Big(u^{n}_{i+\frac{1}{2},j,k} - u^{n}_{i-\frac{1}{2},j,k}\Big)/\Delta x_i;\\
DUR &= \Big(u^{n}_{i+\frac{3}{2},j,k} - u^{n}_{i+\frac{1}{2},j,k}\Big)/\Delta x_{i+1};\\
\Delta x_{\alpha} &= \Delta x_{i+1} - \Delta x_i + \alpha Sign\Big(u_{i+\frac{1}{2},j,k}\Big)(\Delta x_{i+1} - \Delta x_i);\\
VISX &= \mu\left(\frac{u^{n}_{i+\frac{3}{2},j,k} - 2u^{n}_{i+\frac{1}{2},j,k} + U^{n}_{i-\frac{1}{2},j,k}}{\Delta x^2} + \frac{v^{n}_{i,j+\frac{3}{2},k} - 2v^{n}_{i,j+\frac{1}{2},k} + v^{n}_{i,j-\frac{1}{2},k}}{\Delta y^2} + \frac{w^{n}_{i,j,k+\frac{3}{2}} - 2w^{n}_{i,j,k+\frac{1}{2}} + w^{n}_{i,j,k-\frac{1}{2}}}{\Delta z^2}\right)
\end{aligned} \tag{3}$$

where the superscript (n) stands for previous time step, $(n+1)$ for current time step and δt is the time increment. In the above equation, δx, δy and δz are the distance between the center of two adjacent cells in x-, y- and z-directions. Δx, Δy and Δz represent the distance between the faces of two adjacent cells in x-, y- and z-directions.

Node number in x-, y- and z-directions are symbolized by i, j and k, respectively. α is the control factor, where in forward and central differencing has the value of 0 and 1, respectively. Sign is equal to $+1$ if $u_{i+\frac{1}{2}} > 0$ and -1 if $u_{i+\frac{1}{2}} < 0$. A similar method is used for the calculation of advective and viscous flux terms in y- and z-directions.

Conservation of mass (continuity equation) for an incompressible fluid could be written as below

$$\nabla\cdot(\rho\vec{u}) = 0 \tag{4}$$

The finite difference approximation for the continuity equation is

$$D^{n+1}_{i,j,k} = \frac{u^{n+1}_{i+\frac{1}{2},j,k-}u^{n+1}_{i-\frac{1}{2},j,k}}{\rho\delta x_{i+\frac{1}{2}}} + \frac{v^{n+1}_{i,j+\frac{1}{2},k-}v^{n+1}_{i,j-\frac{1}{2},k}}{\rho\delta y_{j+\frac{1}{2}}} + \frac{w^{n+1}_{i,j,k+\frac{1}{2}-}w^{n+1}_{i,j,k-\frac{1}{2}}}{\rho\delta z_{k+\frac{1}{2}}} \tag{5}$$

For satisfaction of the continuity equation, the value of $D^{n+1}_{i,j,k}$ in all cells should be almost zero. The velocities computed according to equation (2) will not, in general, satisfy the continuity equation (equation (5)). To avoid deviation from the mass conservation, the pressure adjustment must be done iteratively (equation (6)). The parameter of δP is defined and added to the pressure given in the previous iteration to modify the value of pressure in each cell. Thus, the velocity values in each direction would be modified and then mass conservation must be checked again

$$\begin{aligned}
\delta p_{i,j,k} &= -\frac{D^{n+1}_{i,j,k}}{2\delta t\left(\frac{1}{\Delta x_i^2} + \frac{1}{\Delta y_j^2} + \frac{1}{\Delta z_k^2}\right)}\\
P^{m+1}_{i,j,k} &= P^{m}_{i,j,k} + \delta p_{i,j,k}\\
u^{m+1}_{i+\frac{1}{2},j,k} &= u^{m}_{i+\frac{1}{2},j,k} + \frac{\delta t}{\delta x}\delta p_{i,j,k}\\
v^{m+1}_{i,j+\frac{1}{2},k} &= v^{m}_{i,j+\frac{1}{2},k} + \frac{\delta t}{\delta y}\delta p_{i,j,k}\\
w^{m+1}_{i,j,k+\frac{1}{2}} &= w^{m}_{i,j,k+\frac{1}{2}} + \frac{\delta t}{\delta z}\delta p_{i,j,k}
\end{aligned} \tag{6}$$

The symbol (m) in the above equations is the number of iterations. After calculation of new velocities, satisfaction of mass conservation (equation (5)) must be investigated again and therefore $D^{n+1}_{i,j,k}$ should be calculated for the whole domain. This iteration process is continued until $D^{n+1}_{i,j,k}$ reach a near zero value (10^{-5} in SUTCAST).

In the filling simulation, the volume of fluid (VOF) method was implemented to track the moving free surface of molten aluminum in the gating system (equation (7)). After solving Navier–Stokes equation and determining the velocity vectors in the whole computational domain, the following equation should be solved

$$\frac{\partial F}{\partial t} + \nabla.\left(\overrightarrow{u}F\right) = 0 \tag{7}$$

In VOF technique, a function $F(x,y,z,t)$ is defined, which is fractional control element occupied by fluid. This function has a range from zero to unity, the cell having F values between 0 and 1 ($0 < F < 1$) represents surface cells, $F = 0$ indicates that the cell contains no fluid (empty spaces) and $F = 1$ corresponds to a cell full of fluid.

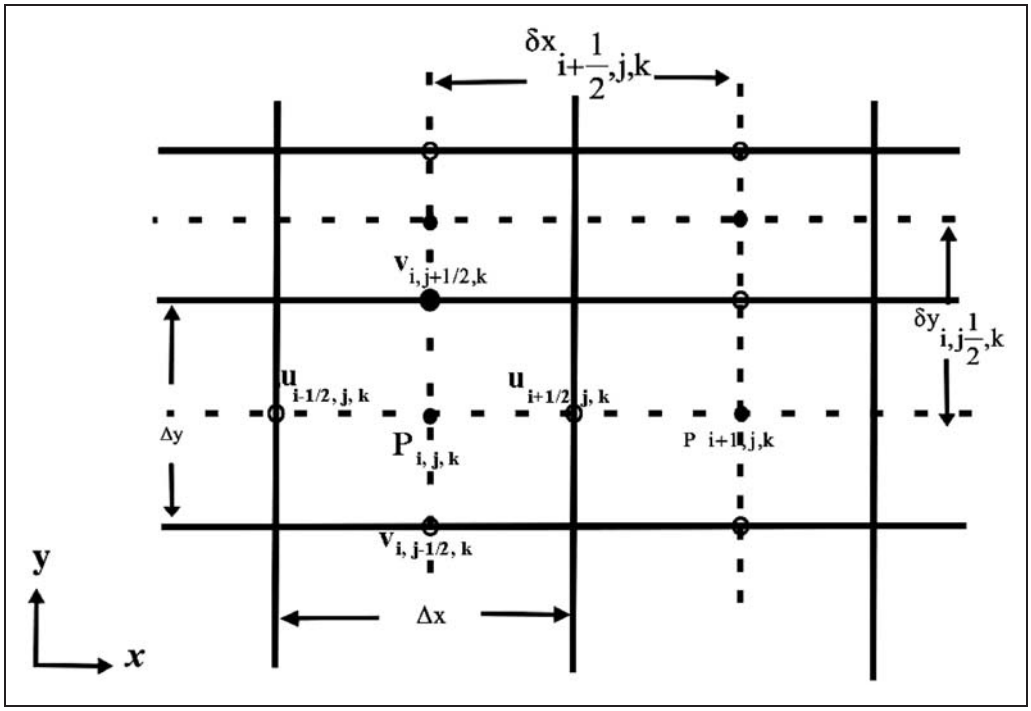

Figure 2. Presentation of velocity and pressure quantities in a computational cell.

Internal boundary condition of no-slip was used to evaluate the effect of mold friction on filling behavior. All the above-mentioned equations were solved on the grids containing cubic mesh. At the curved and tapered boundary conditions, cubic mesh could not fit the geometry completely and the generated meshes appear like steps. This step-like mesh generation in boundary conditions could act as an obstacle against fluid flow and change the direction of melt and cause a back pressure that could have undesirable effects on mold filling. For the purpose of minimizing mesh dependency effects of cubic mesh generation on flow behavior, a mesh refinement was carried out intentionally in the region of sprue base to achieve a nearly smooth boundary condition. The summary of the initial and boundary conditions are shown in Table 2.

Table 2. Initial and boundary conditions.

Model	Pressure inlet (Pa)	Filling time (s)	Total number of cavity meshes
A	1172	2.6	111,006
B	1172	2.62	115,776
C	1172	2.64	123,228
D	1172	2.36	109,503

Results and discussion

Effect of sprue well on filling pattern

In order to evaluate the effects of the geometry of different sprue wells on the filling pattern during mold filling, streamlines at the first time step when liquid metal goes out of the well and enters to the runner were analyzed. Figure 3 shows the streamlines for all sprue wells, which represent the resultant of the velocity in x- and z-directions. Tracing these streamlines in all models, it was observed that in Model A with no sprue well, a small vortex flow was generated at the bottom of the sprue base and this vortex flow was increased with increasing well size while in Model D with a curved sprue base, no vortex flow was observed. The rotation of liquid metals at these points could act as a ball bearing and this pushes the metal into the runner with higher speed. Contours in Figure 3 show the velocity distribution in x-direction, which reaches its maximum value right after the well. Maximum velocity behind the melt front increased when the sprue base increased, that is from 2.9 m s^{-1} in Model D, with curved base, to 4.65 m s^{-1} in Model C, the largest one (Figure 4).

Effect of sprue well on the vena contracta formation

The vena contracta is a widely observed phenomenon in flowing liquids. It occurs wherever a rapid flow is caused to turn through a sharp change of direction. The base of the down runner is probably an even more important example if, as is usually the case, speeds are much higher here. The loss of contact of

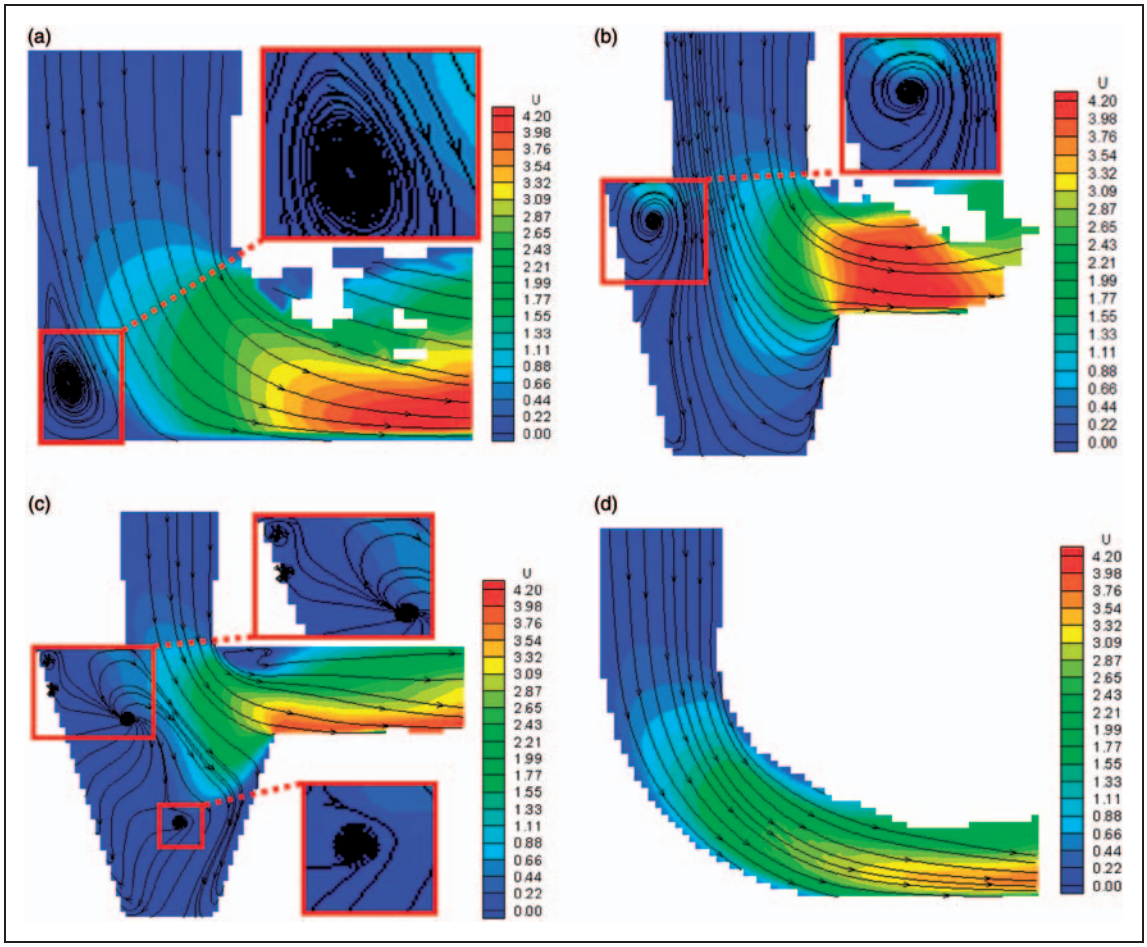

Figure 3. Contours of velocity in the *x*-direction and streamlines in: (a) no sprue well, (b) standard sprue well, (c) large sprue well and (d) curved sprue base.

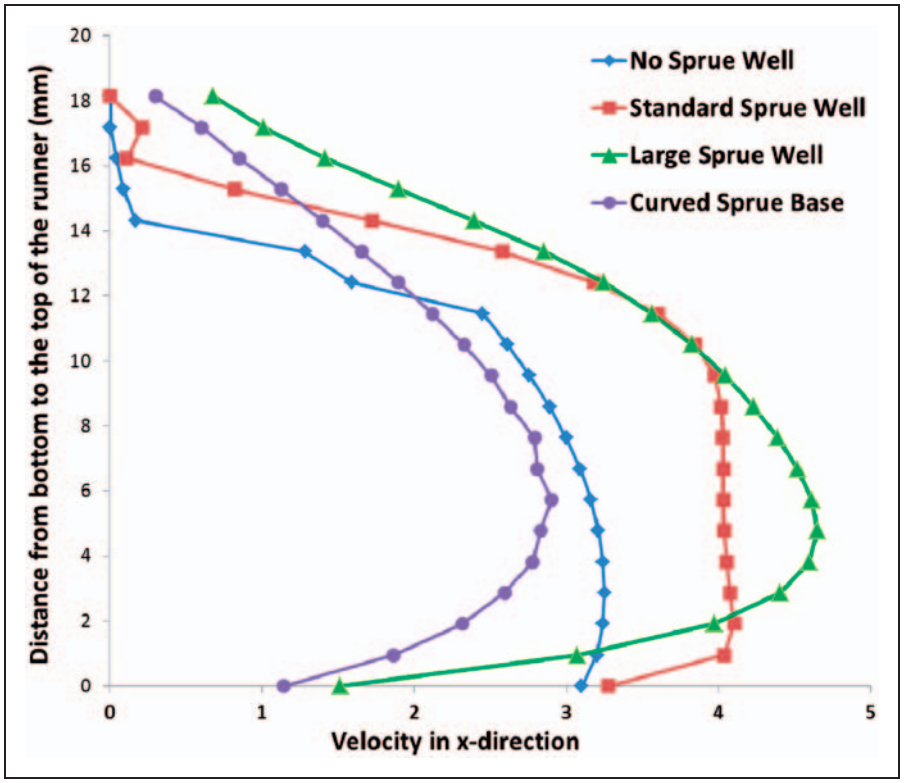

Figure 4. Velocity distribution from top to bottom of the runner.

Table 3. The comparison of *x*-direction velocity (m s^{-1}) in different designs (Models A, B and D) with Model C in different runner positions.

Model	Top	Difference (%)	Middle	Difference (%)	Bottom	Difference (%)
A	0	100	2.75	31.93	3.1	−105.3
B	0	100	3.97	1.73	3.27	−116.55
C	0.67	–	4.04	–	1.51	–
D	0.3	55.22	2.5	38.11	1.14	24.5

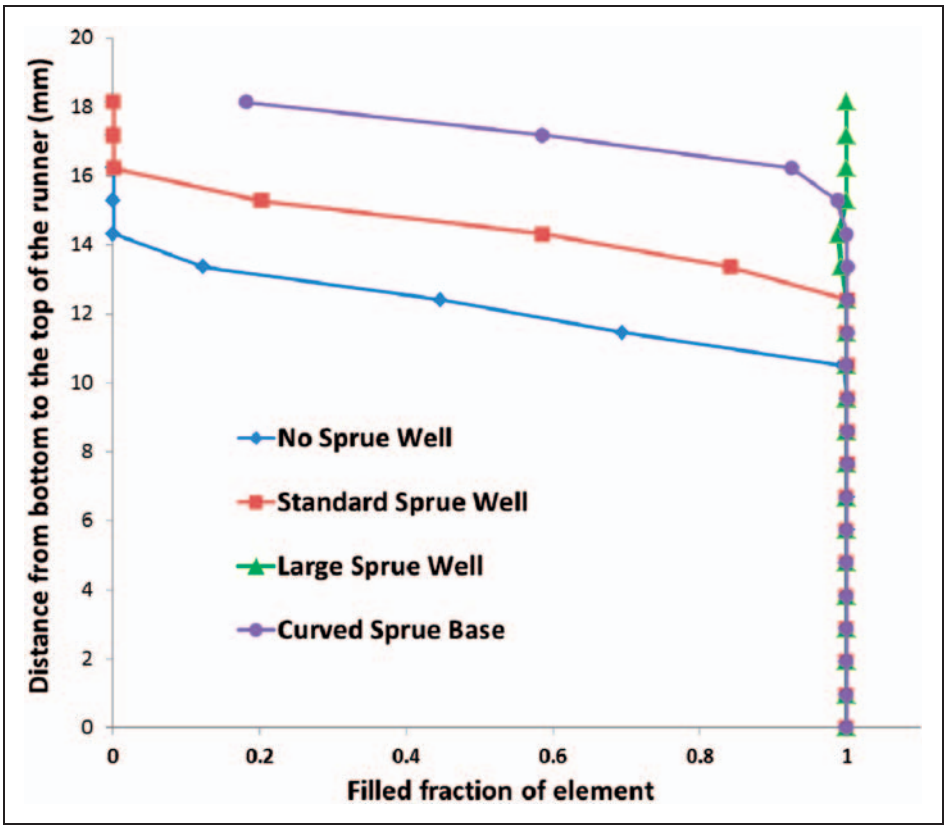

Figure 5. Filled fraction of element with liquid metal.

Table 4. The comparison of filled fraction of element in different designs (Models A, B and D) with Model C in different runner positions.

Model	Top	Difference (%)	Middle	Difference (%)	Bottom	Difference (%)
A	0	100	1	0	1	0
B	0	100	1	0	1	0
C	0.99	–	1	–	1	–
D	0.18	81.81	1	0	1	0

the stream from the top of the runner immediately after the turn has been shown to be the source of much air entrainment in the metal. This is expected to be particularly severe for sand molds, where the permeability will allow a good supply of air to the region of reduced pressure.[2] In order to investigate the contact between liquid metal and runner walls, an attempt was made to predict velocity distribution in the runner right after sprue bases. Figure 4 shows the variation of velocity in the *x*-direction versus distance from the bottom to the top of the runner after sprue base. In Model A where no well was used and in Model B with a standard well, the velocity increases gradually with increasing distance from the top to the bottom of the runner. It is concluded that the contact of liquid metal at the bottom of the runner is much

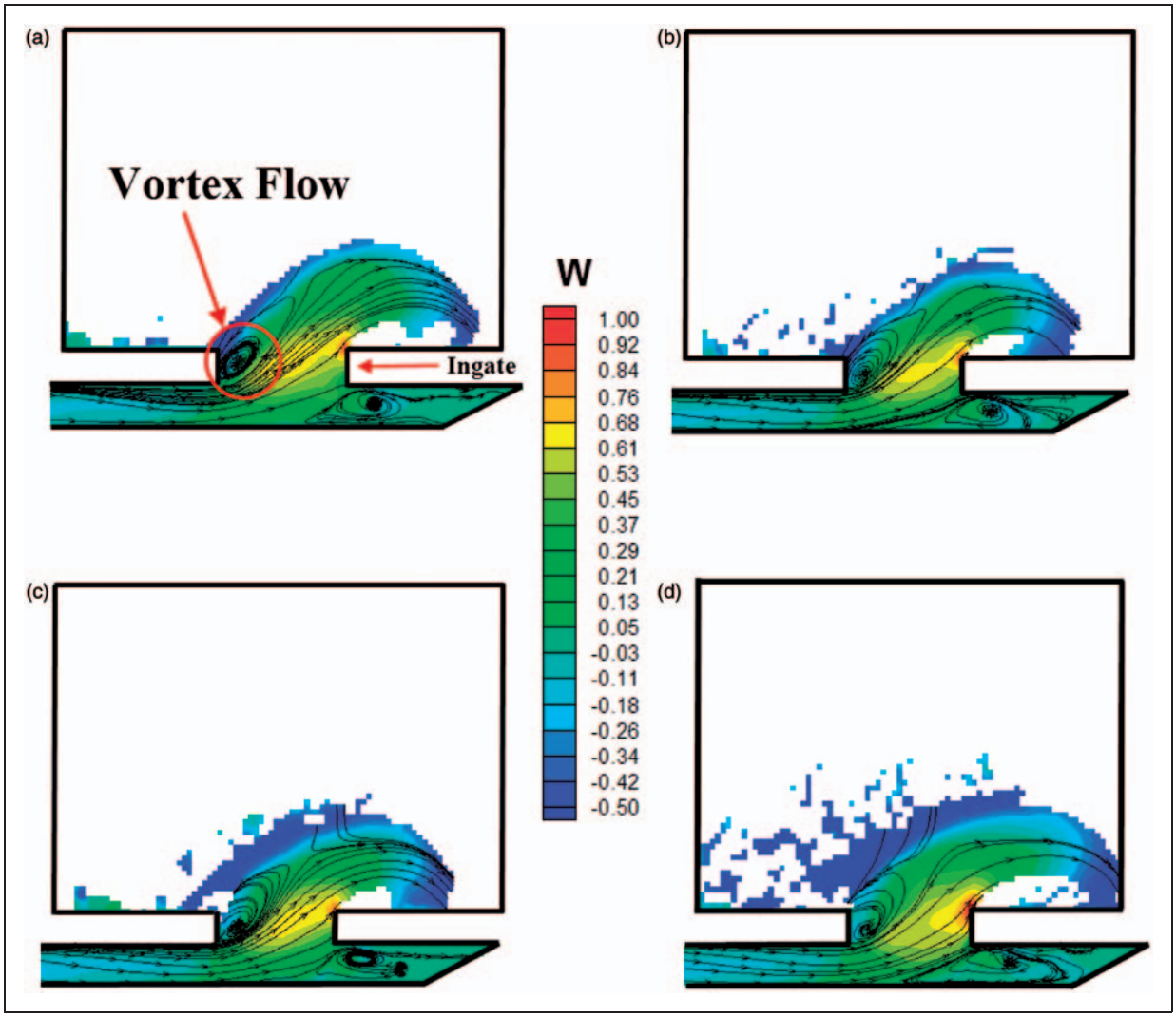

Figure 6. Contours of velocity in z-direction and streamlines in: (a) no sprue well, (b) standard sprue well, (c) large sprue well and (d) curved sprue base.

stronger than that at the top and it will increase the probability of formation of low-pressure zones. From another point of view, the behavior of velocity changes with changing the well size. In contrast to Model A, the velocity reaches its maximum value in more heights in Model C, which has the biggest well. In Model D with a curved sprue base similar to Model C, the velocity in the runner direction reaches its maximum value at the middle of the runner and it depicted that these two types of sprue base could establish a good contact with the runner wall and avoid vena contracta formation. However, it was observed that the average and gradient of velocity in Model C is higher than that of in Model D. It could also lead the casting to higher qualities.

In Table 3, velocity in the x-direction after sprue well in different positions is compared for all models. The velocity at the top of the runner in Model C, with an over-sized well, is much greater than other models, especially Models A and B. It is demonstrated that the probability of formation of low-pressure zone in gating systems where no well were used (Model A) would increase dramatically. But velocity concentration at the bottom of the runner in Models A and B is noticeably higher than in Model C. The negative difference of velocity at the bottom of the runner (−105.3%) confirms that liquid metal in the case where no well was used has complete contact with the bottom of the runner while formation of vena contracta at the top of the runner is inevitable.

The fraction of element that is filled with the liquid at the runner entrance is shown for different sprue base designs in Figure 5, where filled fraction equaling 1 means that the element is fully occupied with liquid and 0 means an empty element. In Models A and B it was found that at the top of the runner there are some empty spaces that contain no or small amount of liquid. Moving from top to bottom of the runner, the fraction of liquid in elements was increased and reached the value of 1. For Model D with a curved sprue base, the fraction of liquid at the first 2 mm of the top of the runner is less than 1. But for Model C with the over-sized well, it shows the value of 1 for the filled fraction at the top of the runner. This shows that

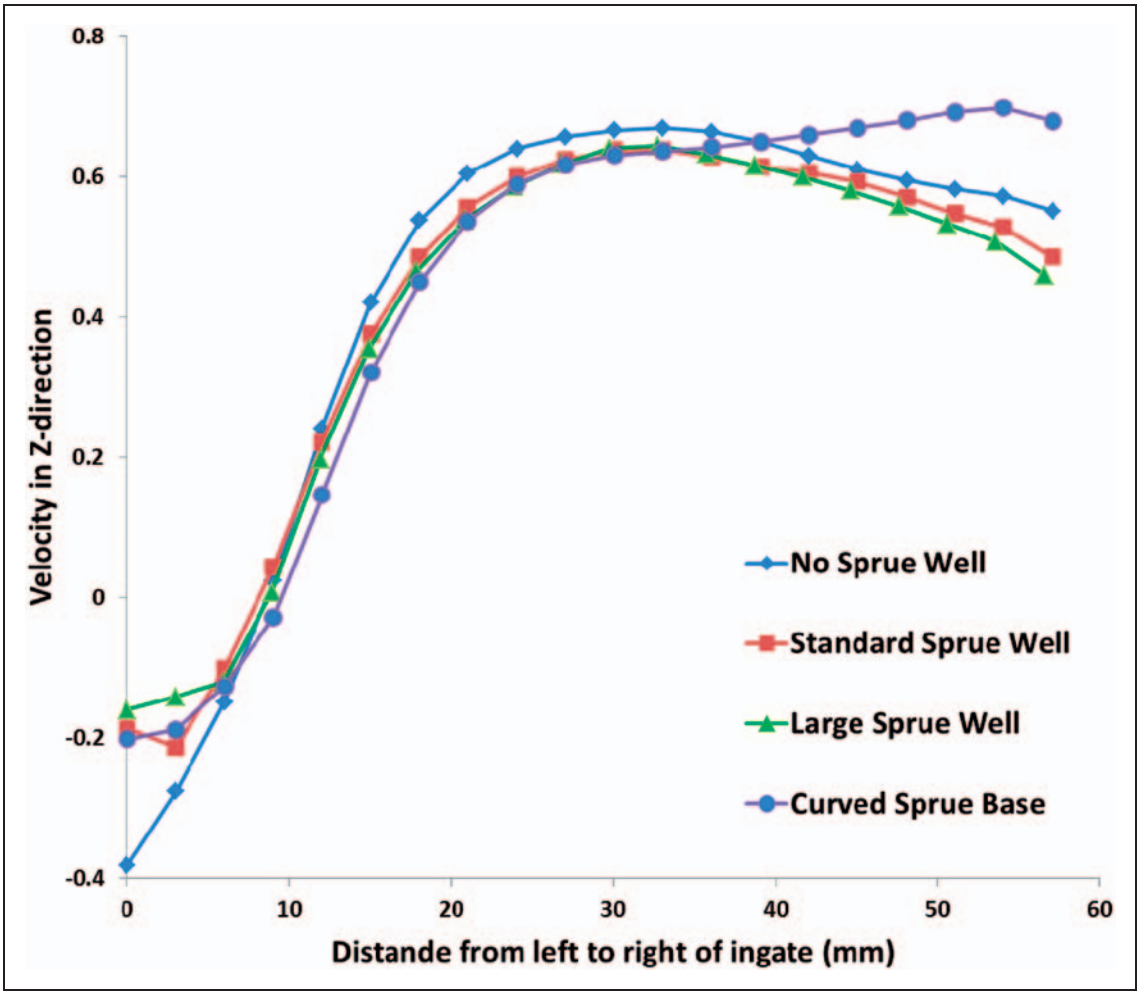

Figure 7. Velocity distribution in z-direction from left side of ingate to the right side at the middle of ingate.

although both Models C and D made good contact with the runner wall, the most perfect contact with the runner wall was observed in Model C with an oversized well.

In Table 4 the comparison of filled fraction of element with liquid metal in different positions of runner is presented for different models of sprue bases. It is easy to understand that with increasing distance from the top of the runner to the bottom, the volume fraction of elements that are occupied with liquid increases for Model A where there is no well and Model B where a standard sprue well was used. The maximum filled fraction of element at the top of the runner for Model D, using curved sprue base, is 0.18 and this increase to 1 when we moved down only by 2 mm from the top of the runner. This shows that after Model C, which filled the runner and made good contact with the runner wall, Model D could also be a good alternative for removing vena contracta.

Effect of sprue base on ingate velocity

The sizing of the gates should be provided with sufficient area to reduce the velocity of the melt below the critical value of 0.5 m s^{-1} to keep avoiding the formation of surface turbulence and hence entrainment of oxide films. In order to evaluate how a sprue well could affect ingate velocity, the distribution of the velocity in the *z*-direction the first time when liquid metal fills the gate and enters the cavity was analyzed (Figure 6). The velocity distribution in all cases is nearly similar. Although it was supposed that the melt could fill the ingate completely, it was observed that only the right portion of the ingate is filled.

Maximum velocity (0.7 m s^{-1}) was seen at the right corner of the ingate end, which exceeded the critical velocity. Vortex flow was observed in the left side of the ingate. The rotation of liquid here pushes the molten metal back into the runner and prevents the melt from entering into the mold cavity. Negative velocities in this region are because of downward motion of liquid metal. As some parts of the ingate are occupied by vortex flow, the effective ingate area reduces, causes the velocity to increase and finally exceed the critical velocity. Figure 6 proves that filling pattern in the ingate is the same for all the Models (A–D) and does not depend on to the sprue base design. Therefore, exceeding critical velocity in the ingate and surface

turbulence generation is not associated with the sprue base design.

Velocity in z-direction at the middle of ingate is depicted in Figure 7. Here negative values on the left side of the ingate imply that no molten metal is eligible to pass through this region to the mold cavity. A steep increase in velocity was observed while moving towards the right side of the ingate but it became constant after 20 mm distance from the left side. The maximum velocity in z-direction was about 0.7 m s^{-1}, which exceeded the critical value. About 60% of gate area remained at this higher velocity while the rest experienced a lower one. It is clear that here the effective area is obviously smaller than that expected and this lead to exceeds critical ingate velocity and splashing of melt into the mold cavity. It could be concluded that in this case, with this specific geometry, although the velocity in the runner is affected by well size, the ingate velocity is more influence by other casting considerations such as ingate geometry and location.

Conclusion

Effects of employing different sprue bases (no well, standard, large wells and curved sprue base) have been investigated by CFD in this study. The following are the conclusions:

1. It was found that locating the sprue well in gating systems, especially larger ones, increases the possibility of formation of vortex flow in sprue base, which leads to an increase in surface turbulence and therefore entrainment defects.
2. Maximum velocity behind the melt front increased when the sprue size increased, that is from 2.9 m s^{-1} in Model D, with curved base, to 4.65 m s^{-1} in Model C, the largest one.
3. Rather large wells (Model C) could eliminate vena contracta while keeping a full contact between the runner wall and liquid metal.
4. Curved sprue base (Model D) produced no vortex flow at the bottom of the sprue with a nearly full contact between the runner wall and liquid metal (only 2 mm from the top of the runner is empty in this model). Liquid metal has experienced the lowest velocity (2.9 m s^{-1}) at the runner in this design.
5. Ingate velocity was observed to be nearly the same for all sprue base systems. By moving from the left to the right of the ingate, the z velocity in all models has a range from a negative value to 0.7 m s^{-1}. It was demonstrated that ingate velocity depends on other casting considerations such as distance between sprue and gates, gating system geometry and ratio.

Funding

This research received no specific grant from any funding agency in the public, commercial, or not-for-profit sectors.

References

1. Elliot R. *Cast iron technology*. Oxford, UK: Butterworths-Heinemann, 1988.
2. Campbell J. *Castings practice: the 10 rules of castings*. Oxford, UK: Butterworth-Heinemann, 2004.
3. Campbell J and Runyoro J. The running and gating of light alloys. *Foundaryman* 1992; 85: 117–124.
4. Kura JG and Grube KR. Principles applicable to vertical gating. *Trans Am Foundry Soc* 1955; 63: 35–48.
5. Campbell J and Green NR. Statistical distributions of fracture strengths of cast Al-7Si-Mg alloy. *Mater Sci Eng A* 1993; 173: 261–266.
6. Campbell J and Green NR. Influence of oxide film filling defects on the strength of Al-7Si-Mg alloy casting. *Trans Am Foundry Soc* 1994; 102: 341–347.
7. Campbell J. *Castings*. 2nd ed. Oxford, UK: Butterworth-Heinemann, 1991.
8. Barkhudarov MR and Hirt CW. Casting simulation: mold filling and solidification- benchmark calculations using FLOW-3D(R). Technical report, Flow Science Inc, Los Alamos, New Mexico, 1993.
9. Barkhudarov MR and Williams K. Simulation of surface turbulence, fluid flow during mold filling. *Trans Am Foundry Soc* 1995; 95–90 and 669–674.
10. Dai X, Yang X, Campbell J, et al. Effects of runner system design on the mechanical strength of Al-7Si-Mg alloy castings. *Mater Sci Eng A* 2003; 354: 315–325.
11. Hashemi H and Raiszadeh R. Naturally-pressurized systems: the role ceramic filter. *J Appl Sci* 2009; 9(11): 2115–2122.
12. Hsu F and Lin H. A diffusing runner for gravity casting. *Metal Mater Trans B* 2009; 40B: 833–842.
13. Masoumi M, Hu H, Hedjazi J, et al. Effect of gating design on mold filling. In: *AFS Transactions 2005*, Schaumburg, IL, 16–19 April 2005, paper no. 05-152(02), pp. 1–12. Schaumburg, IL: American Foundry Society.
14. Webster PD and Met M. Study of the flow of metals in runners. *Br Foundryman* 1967; 60: 314–319.
15. Schwam D, Wallace JF, Engle T, et al. Gating of permanent molds for aluminum castings. Final technical report, Department of Materials Science, Case Western Reserve University, Cleveland, OH, 2004.
16. Shabani MO and Mazahery A. Computational fluid dynamics (CFD) simulation of liquid-liquid mixing in mixer settler. *Arch Metallurgy Mater* 2012; 57(1): 173–178.

17. Mirbagheri SMH, Dadashzadeh M, Serajzadeh S, et al. Modeling the effect of mould wall roughness on the melt flow simulation in casting process. *Appl Math Model* 2004; 28: 933–956.
18. Shabani MO and Mazahery A. Evaluation of the effect of mixer settler baffles on liquid-liquid extraction via CFD simulation. *UPB Sci Bull Ser D* 2011; 73(4): 55–64.
19. Hirt CW and Nichols BD. Volume of fluid (VOF) method for the dynamic of free boundaries. *J Comput Phys* 1981; 39: 201–225.
20. Shabani MO, Mazahery A, Alizadeh M, et al. Computational fluid dynamics (CFD) simulation of effect of baffles on separation in mixer settler. *Int J Mining Sci Technol* 2012; 22: 703–706.